IET Power Electronics

Avoiding overvoltage problems in three-phase distributed-generation systems during unbalanced voltage sags

PEL-2019-1178.R1 | Research Article

Submitted on: 17-01-2020

Submitted by: Miguel Castilla, Antonio Camacho, Jaume Miret, Ramon Guzman, Luis Garcia de Vicuna

Keywords: THREE-PHASE INVERTER, DISTRIBUTED POWER GENEARTION, VOLTAGE SAGS, CURRENT LIMITERS

Avoiding overvoltage problems in three-phase distributed-generation systems during unbalanced voltage sags

Miguel Castilla [1*], Antonio Camacho [2], Jaume Miret [1], Ramón Guzmán [2], Luis García de Vicuña [1]

[1] Electronic Engineering Department, Technical University of Catalonia, Vilanova i la Geltrú, Spain
[2] Automatic Control Department, Technical University of Catalonia, Vilanova i la Geltrú, Spain
[*] miquel.castilla@upc.edu

Abstract: During voltage sags, distributed generation systems must fulfil specific grid-code requirements for reactive current injection. This ancillary service can produce overvoltage problems in networks operating in unbalanced conditions when the amplitude of one of the phase voltages is higher than the others and a balanced reactive current is injected through a large grid impedance. This paper proposes a control scheme to avoid these overvoltage problems, thus reducing the risk of cascade disconnection that this incident may produce. The derivation of the control scheme starts from the flexible oscillating-power control, introduces the necessary modifications so that this control meets the grid-code requirements for current injection and combines it with a slope voltage control to achieve a good voltage regulation. A theoretical analysis is included to determine the expressions that quantify the voltage support characteristics of the proposal. Finally, selected experimental results are reported to validate the characteristics of the proposed control.

1 Introduction

Distributed generation (DG) systems are continually exposed to the disturbances existing in the utility grid. A critical disturbance is a short circuit fault, which typically produces a voltage sag in the network [1, 2]. In this scenario, DG systems drastically deteriorate their operation, especially during unbalanced voltage sags [3, 4]. In the last decade, different control strategies have been developed to improve the performance of DG systems during these critical disturbances. The basic strategies can be classified as [5-7]

1) Constant active power control ($k = 1$).
2) Constant reactive power control ($k = -1$).
3) Balanced current control ($k = 0$).
4) Flexible oscillating-power control ($-1 \leq k \leq 1$).

For these strategies, the value of the control parameter k identifies the way in which the active and reactive power supplied by the DG system is injected via positive- and negative-sequence components and, consequently, it defines the particular characteristics of the strategies. The common characteristics are the presence of power oscillations at twice the grid frequency and the injection of unbalanced current. In particular, the first strategy has the ability to eliminate the oscillations in the active power, the second one removes the oscillations in the reactive power, and the third one injects balanced current [7]. The last control strategy is a generalization of the previous ones. Its characteristics can be adjusted online by modifying the value of k inside its allowed range. Apart from being able to reproduce the operation of the first three strategies, it can also operate with intermediate characteristics between these strategies [6, 7]. In this way, this strategy can be designed to perform an additional goal, thus enhancing their advantages over the other basic strategies.

Recently, advanced control strategies with new features have been introduced to guarantee their use in practical applications [8, 9]. The first additional feature is the fulfilment of the grid code requirements for current injection during voltage sags [10, 11]. This feature is directly related to the mechanism of reactive current injection [12, 13]. The second one is the limitation of the peak current to prevent overcurrent in the DG system [14, 15]. The design of the current limitation technique in the balanced current control is simple, as it can be seen in [16]. However, in the constant active power control, the application of the peak-current limitation is more complicated due to the presence of positive- and negative-sequence current components [17-19]. As far as the authors know, both the constant reactive power control and the flexible oscillating-power control have not been equipped with a peak-current limitation mechanism in the literature.

In three-phase DG systems, the controllability of the current has four degrees of freedom under unbalanced voltage conditions [20]. In the basic control strategies, the four degrees of freedom are used to define the characteristics of the power injection. In particular, each strategy is able to set both the mean value and the amplitude of the oscillation of the active and reactive powers in a different way [7]. In the advanced control strategies, the priority moves towards the injection of the current according to the requirements of the grid code and to limit the maximum peak current [19]. In these strategies, the injected active power may experience a curtailment if the maximum current exceeds its allowed limit since the injection of the generated power is no longer one of the priorities of the control. In this sense, it is interesting to analyse the response of the DG system against other characteristics when the four degrees of freedom have been assigned a priori, as described above. A focus of interest is the evaluation of the ability of the advanced control strategies to avoid overvoltage during voltage sags [21, 22]. The overvoltage problem is favoured in networks operating in unbalanced conditions when the amplitude of one of the phase voltages is clearly higher than the others and a balanced current is injected though a large grid impedance [23, 24]. In this sense, the injection of unbalanced currents seems to be the best option [25, 26]. The relevance of this analysis is that it tries to prevent the risk of overvoltage and the consequent cascade disconnection of DG systems that this incident may produce. The impact of flexible oscillating-power control on

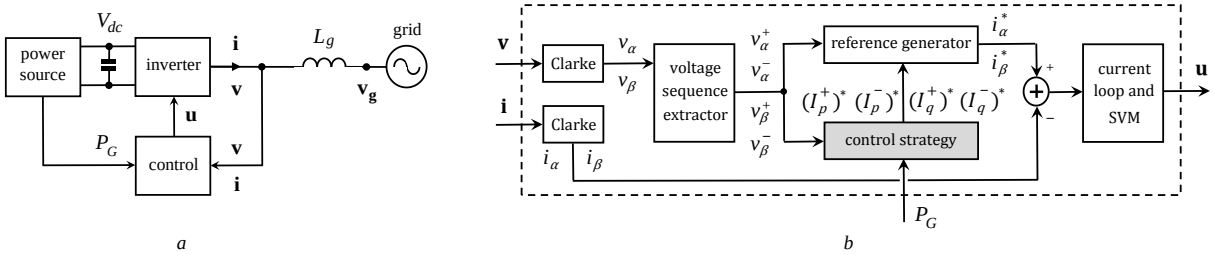

Fig. 1 *Three-phase DG system*
(a) Single-line diagram, ***(b)*** control diagram

system overvoltage has not been previously studied in the literature.

To conclude with the analysis of the state-of-the-art for DG systems under voltage sags, it is worth noting that the control strategies devised for this application typically operate in open loop. This issue can be clearly seen in the review papers [6, 7]. However, the closed-loop operation allows to better exploit these systems and extract their most outstanding characteristics.

This paper presents an advanced flexible oscillating-power control with grid-code current injection and peak-current limitation. This control scheme can reproduce the operation of the constant active power control, constant reactive power control, balanced current control, and it can also operate with intermediate characteristics between these controls. An analysis is included to determine the theoretical expressions of the maximum amplitude of the phase voltages, revealing its dependence with the parameter *k*. A closed-loop slope voltage control is introduced to calculate online the value of this parameter in order to avoid the overvoltage problem. The contributions of this study are validated by experimental results and are listed below:

1) A flexible oscillating-power control providing grid-code current injection and peak-current limitation.
2) Analytical expressions of the maximum amplitude of the phase voltages as a function of the inputs of the flexible oscillating-power control.
3) A closed-loop slope voltage control that prevents the overvoltage problem.

The rest of the paper is organised as follows. In Section 2, the DG system under study is described. In Section 3, an advanced flexible oscillating-power control is presented, including the pseudocode of the proposed algorithm. In Section 4, the overvoltage problem is analysed and the voltage support properties of the proposed strategy are revealed. In Section 5, a closed-loop controller to prevent the overvoltage problem is introduced, including control design guidelines. Section 6 presents selected experimental results. Section 7 compares the characteristics of the proposed control with those of the state-of-the-art control solutions. Section 8 concludes the paper.

2 System description

2.1 DG system

Fig. 1a shows the single-line diagram of the three-phase DG system considered in this study. It is formed by a power source, a dc-link capacitor, a power inverter, and a control scheme. The inverter injects the current **i** to the grid, synchronized with the voltage **v**. The grid is modelled by the series connection of the inductor L_g and the voltage source $\mathbf{v_g}$. This is the typical model of a high- or medium-voltage grid with a dominant inductive impedance ($X/R \gg 1$) [8, 15, 23]. The control measures **v** and **i**, receives the power generated by the power source P_G and provides the signal **u** to drive the switches of the inverter.

Fig. 1b shows the diagram of the control scheme. It is formulated in $\alpha\beta$ stationary frame. The inputs **v** and **i** are converted to $\alpha\beta$ signals using Clarke transformation. The voltage sequence extractor behaves as a narrow band-pass filter and estimates the positive- and negative sequence components of the fundamental (first harmonic) $\alpha\beta$ voltages [27, 28]. Due to this filtering action, the voltages and currents in the control scheme are free of harmonics and, as a consequence, these external disturbances (grid harmonics) do not affect the operation of the control scheme.

The control strategy block is the key element in the control scheme. It is responsible to calculate the amplitudes of the reference currents according to the specific control objectives. The meaning of these control variables are

- $(I_p^+)^*$: Amplitude of the positive-sequence component of the reference active current.
- $(I_p^-)^*$: Amplitude of the negative-sequence component of the reference active current.
- $(I_q^+)^*$: Amplitude of the positive-sequence component of the reference reactive current.
- $(I_q^-)^*$: Amplitude of the negative-sequence component of the reference reactive current.

The control objectives are described in the next subsection.

The reference generator in Fig. 1b calculates the instantaneous reference currents using the amplitudes of the reference currents and the sequence voltages [19]

$$i_\alpha^* = \frac{v_\alpha^+}{V^+}(I_p^+)^* + \frac{v_\alpha^-}{V^-}(I_p^-)^* + \frac{v_\beta^+}{V^+}(I_q^+)^* + \frac{v_\beta^-}{V^-}(I_q^-)^* \quad (1)$$

$$i_\beta^* = \frac{v_\beta^+}{V^+}(I_p^+)^* + \frac{v_\beta^-}{V^-}(I_p^-)^* - \frac{v_\alpha^+}{V^+}(I_q^+)^* - \frac{v_\alpha^-}{V^-}(I_q^-)^* \quad (2)$$

where V^+ and V^- are the amplitudes of the positive- and negative-sequence voltages, respectively,

$$V^+ = \sqrt{(v_\alpha^+)^2 + (v_\beta^+)^2} \quad (3)$$

$$V^- = \sqrt{(v_\alpha^-)^2 + (v_\beta^-)^2}. \quad (4)$$

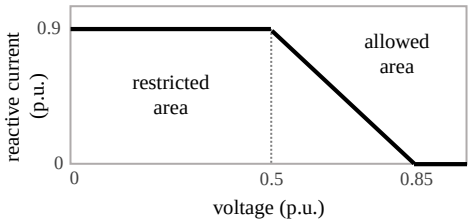

Fig. 2 *Specification of reactive current injection for wind farms during voltage sags in the Spanish grid code*

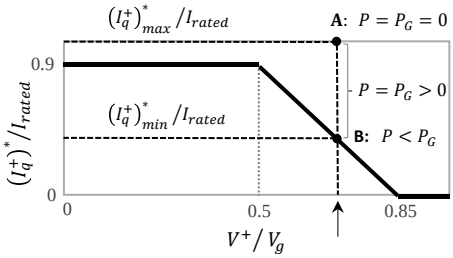

Fig. 3 *Allowed variation of the positive-sequence component of the reference reactive current*

To finalize with the description of Fig. 1b, the current control loop and the space vector modulator (SVM) generate the driving signal **u**. The compensators used in the control loop are based on proportional and resonant integrators to guarantee an accurate tracking of the sinusoidal reference currents in the $\alpha\beta$ channels [29, 30].

2.2 Control objectives

In the considered DG system, the control of the current has four degrees of freedom [20]. During voltage sags, this allows to define the following four control objectives taking in mind the nature of the considered grid with a dominant inductive impedance ($X/R \gg 1$)

1) Prevent overcurrent by ensuring that the maximum current I_{max} does not exceed the rated current of the power inverter I_{rated}

$$I_{max} \leq I_{rated} \tag{5}$$

where

$$I_{max} = \max(I_a, I_b, I_c) \tag{6}$$

and I_a, I_b, I_c are the amplitudes of the phase currents.

2) Fulfil the grid-code requirements for reactive current injection

$$\left(I_q^+\right)^* \geq \left(I_q^+\right)^*_{min} \tag{7}$$

where $\left(I_q^+\right)^*_{min}$ is the minimum amplitude of the positive-sequence component of the reference reactive current specified by the grid code.

3) Inject the power generated by the power source P_G.

4) Avoid overvoltage problems by forcing that the maximum voltage V_{max} does not exceed the upper allowed limit V_U

$$V_{max} \leq V_U \tag{8}$$

where

$$V_{max} = \max(V_a, V_b, V_c) \tag{9}$$

and V_a, V_b, V_c are the amplitudes of the phase voltages. In this paper, $V_U = 1.1$ p. u. is considered.

3 Flexible oscillating-power

This Section presents an advanced flexible oscillating-power control that fulfils the control objectives 1, 2 and 3. This is the first contribution of this paper.

3.1 Grid code requirements for current injection

Grid codes provide technical requirements for the operation of grid-connected systems during voltage sags. For interested readers, a review of different grid codes can be found in [31, 32]. In this study, the Spanish grid code for wind farms is considered [11]. The requirements for reactive current injection of this code are presented below.

First, the DG system must inject the rated current of the power inverter I_{rated} during the voltage sag. This particular requirement satisfies the control objective 1, as follows

$$I_{max} = I_{rated} \tag{10}$$

Second, the DG system must inject at least the minimum reactive current specified in [11]. Fig. 2 shows this current as a function of the output voltage. For the derivation of the control proposed in this section, the minimum current specification is adapted by considering positive-sequence components for both the reference reactive current and the output voltage. In this case, the minimum current can be written as

$$\left(I_q^+\right)^*_{min} = \begin{cases} 0 & V^+ \geq 0.85 \\ 2.19 - 2.57V^+ & 0.5 < V^+ < 0.85 \\ 0.9 & V^+ \leq 0.5 \end{cases} \tag{11}$$

In (11), the reactive current and the voltage are expressed in p.u. The base values are I_{rated} and V_g, the latter being the nominal grid voltage. During the voltage sag, the reference reactive current must be positioned in the allowed area of Fig. 2, by satisfying the control objective 2 expressed in (7).

Fig. 3 shows an example of the variation of the reactive current. For the particular value of V^+ indicated by the arrow, the line between the points A and B denotes the allowed values of the reactive current. The point A corresponds to the maximum reactive current when $P_G = 0$. The operating points are going down the line as P_G increases. The point B corresponds to the minimum reactive current. The system remains at this point making the power injected by the inverter lower than that generated by the power source. This fact is known as active power curtailment and happens due to the limitation of the maximum injected current, as indicated in (10).

3.2 Current limitation technique

The technique for current limitation is based on imposing (10)

Table 1 Advanced flexible oscillating-power control

$(I_q^+)^* > (I_q^+)^*_{min}$	$(I_p^+)^*$	$(I_q^+)^*$	$(I_p^-)^*$	$(I_q^-)^*$
yes	$\frac{2}{3}\frac{P_G}{V^+}\frac{1}{1-kn^2}$	$\sqrt{\frac{I_{rated}^2}{1-2knc_k+(kn)^2}-\left((I_p^+)^*\right)^2}$	$-kn(I_p^+)^*$	$kn(I_q^+)^*$
no	$\sqrt{\frac{I_{rated}^2}{1-2knc_k+(kn)^2}-\left((I_q^+)^*_{min}\right)^2}$	$(I_q^+)^*_{min}$	$-kn(I_p^+)^*$	$kn(I_q^+)^*$

for any possible value of I_{max}. In [19], this current was obtained for the advanced constant active power control as

$$I_{max} = (I^+)^*\sqrt{1-2nc_{min}+n^2} \tag{12}$$

where

$$(I^+)^* = \sqrt{\left((I_p^+)^*\right)^2+\left((I_q^+)^*\right)^2} \tag{13}$$

$$c_{min} = \min\left(\cos\varphi, \cos\left(\varphi-\frac{2\pi}{3}\right), \cos\left(\varphi+\frac{2\pi}{3}\right)\right) \tag{14}$$

$$\cos\varphi = \frac{v_\alpha^+ v_\alpha^- - v_\beta^+ v_\beta^-}{V^+V^-} \tag{15}$$

$$\sin\varphi = \frac{v_\alpha^+ v_\beta^- + v_\alpha^- v_\beta^+}{V^+V^-} \tag{16}$$

$$n = \frac{V^-}{V^+}. \tag{17}$$

By selecting c_{min} as in (14), the current I_{max} really takes its maximum value; see the impact of c_{min} in I_{max} in (12).

For the proposed flexible oscillating-power control, the value of I_{max} is derived by including the parameter k in (12)

$$I_{max} = (I^+)^*\sqrt{1-2knc_k+(kn)^2} \tag{18}$$

where

$$c_k = \begin{cases} c_{min}, & \text{for } k \geq 0 \\ c_{max}, & \text{for } k < 0 \end{cases} \tag{19}$$

$$c_{max} = \max\left(\cos\varphi, \cos\left(\varphi-\frac{2\pi}{3}\right), \cos\left(\varphi+\frac{2\pi}{3}\right)\right) \tag{20}$$

Note that I_{max} takes its maximum value by minimizing or maximizing c_k according to the sign of k shown in (20).

3.3 Amplitudes of the reference currents

This subsection derives the amplitudes of the reference currents for the advanced flexible oscillating-power control.

By replacing (10) in (18), the current $(I^+)^*$ can be written as

$$(I^+)^* = \frac{I_{rated}}{\sqrt{1-2knc_k+(kn)^2}} \tag{21}$$

This expression is valid for all operating points shown in Fig. 3, from A to B, regardless of whether there is active power curtailment or not.

The expressions of $\left(I_p^+\right)^*$ and $\left(I_q^+\right)^*$ are obtained from (13) and (21), according to the result of evaluating (7). The results

FUNC: $\left((I_p^+)^*, (I_p^-)^*, (I_q^+)^*, (I_q^-)^*\right)$ = Control Strategy $\left(v_\alpha^+, v_\alpha^-, v_\beta^+, v_\beta^-, P_G\right)$

/* Amplitudes and phase of the sequence voltages: (3),(4), (15)-(17) */
$V^+ = \text{sqrt}\left((v_\alpha^+)^2 + (v_\beta^+)^2\right)$
$V^- = \text{sqrt}\left((v_\alpha^-)^2 + (v_\beta^-)^2\right)$
$n = V^-/V^+$
$\cos\varphi = \left(v_\alpha^+ v_\alpha^- - v_\beta^+ v_\beta^-\right)/(V^+V^-)$
$\sin\varphi = \left(v_\alpha^+ v_\beta^- + v_\alpha^- v_\beta^+\right)/(V^+V^-)$
/* Calculation of c_k: (14), (19), (20) */
$c_{min} = \min(\cos\varphi, \cos(\varphi-2\pi/3), \cos(\varphi+2\pi/3))$
$c_{max} = \max(\cos\varphi, \cos(\varphi-2\pi/3), \cos(\varphi+2\pi/3))$
if $k \geq 0$ **then** $c_k = c_{min}$ **else** $c_k = c_{max}$ **end**
/* Amplitude of the minimum reference reactive current: (11) */
if $V^+/V_g \geq 0.85$ **then** $(I_q^+)^*_{min} = 0$ **end**
if $0.5 < V^+/V_g < 0.85$ **then** $(I_q^+)^*_{min} = (2.19 - 2.57V^+)\, I_{rated}$ **end**
if $V^+/V_g \leq 0.5$ **then** $(I_q^+)^*_{min} = 0.9\, I_{rated}$ **end**
/* Amplitudes of the reference currents: Table 1 */
$(I_p^+)^* = (2/3)\, P_G/\left(V^+(1-kn^2)\right)$
$(I_q^+)^* = \text{sqrt}\left(I_{rated}^2/(1-2knc_k+(kn)^2) - \left((I_p^+)^*\right)^2\right)$
if $(I_q^+)^* < (I_q^+)^*_{min}$ /* Active power curtailment: $P < P_G$ */
  then $(I_q^+)^* = (I_q^+)^*_{min}$
  $(I_p^+)^* = \text{sqrt}\left(I_{rated}^2/(1-2knc_k+(kn)^2) - \left((I_q^+)^*_{min}\right)^2\right)$
end
$(I_p^-)^* = -kn(I_p^+)^*$
$(I_q^-)^* = kn(I_q^+)^*$

Fig. 4 *Pseudocode of the proposed flexible oscillating-power control*

are shown in Table 1. When there is no power curtailment, the control objective 3 is satisfied and the active current $\left(I_p^+\right)^*$ is calculated according to the generated power P_G. In addition, the reactive current is responsible to limit the maximum current to I_{rated}. When there is power curtailment, the reactive current takes its minimum value according to the grid-code requirement and the role of limiting the maximum current is then assumed by the active current. In any case, the negative-sequence currents have the same expressions that in the basic flexible oscillating-power control [7]. Finally, note that the flexibility in the proposed control scheme is given by the fact that the amplitudes of the reference currents depend on the control parameter k, as it can be seen in Table 1. Thus, different characteristics can be obtained by varying k inside its allowed range.

3.4 Control algorithm

Fig. 4 shows the pseudocode that implements the algorithm of the proposed flexible oscillating-power control. The inputs

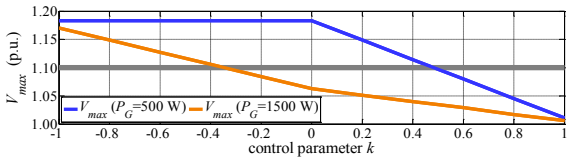

Fig. 5 *Merit factor V_{max} as a function of the control parameter k for two values of P_G*

of the algorithm are the sequence voltages and the power generated by the power source. The outputs are the amplitudes of the reference sequence currents. The variables k, V_g and I_{rated} must be declared and initialized at the beginning of the main code.

4 Voltage support properties

This Section reveals the voltage support properties of the advanced flexible oscillating-power control. For this purpose, the expressions to calculate V_{max} as a function of the inputs of this control scheme are first derived and then the influence of the parameter k on this factor is discussed. This analysis is the second contribution of this paper.

From Fig. 1a and assuming an accurate tracking of the reference current $\mathbf{i}^*$ (i.e., $\mathbf{i} = \mathbf{i}^*$) [29], the output voltage $\mathbf{v}$ of the DG system can be expressed as

$$\mathbf{v} = \mathbf{v_g} + L_g \frac{d\mathbf{i}^*}{dt}. \tag{22}$$

In this case, the amplitudes of the phase voltage components of $\mathbf{v}$ can be expressed as [33]

$$V_a = V_{ga} + \omega L_g I_{qa}^* \tag{23}$$

$$V_b = V_{gb} + \omega L_g I_{qb}^* \tag{24}$$

$$V_c = V_{gc} + \omega L_g I_{qc}^* \tag{25}$$

being V_{ga}, V_{gb}, V_{gc} the amplitudes of the phase voltages of $\mathbf{v_g}$, and I_{qa}^*, I_{qb}^*, I_{qc}^* the amplitudes of the reactive phase current components of $\mathbf{i}^*$. These current components can be written as a function of the amplitudes of the symmetrical components as (see the Appendix for a detailed derivation)

$$I_{qa}^* = \frac{Q_t^* + Q_o^* \cos\varphi + Q_i^* \sin\varphi}{V_a} \tag{26}$$

$$I_{qb}^* = \frac{Q_t^* + Q_o^* \cos\left(\varphi - \frac{2\pi}{3}\right) + Q_i^* \sin\left(\varphi - \frac{2\pi}{3}\right)}{V_b} \tag{27}$$

$$I_{qc}^* = \frac{Q_t^* + Q_o^* \cos\left(\varphi + \frac{2\pi}{3}\right) + Q_i^* \sin\left(\varphi + \frac{2\pi}{3}\right)}{V_c} \tag{28}$$

where

$$Q_t^* = V^+\left(I_q^+\right)^* - V^-\left(I_q^-\right)^* \tag{29}$$

$$Q_o^* = V^-\left(I_q^+\right)^* - V^+\left(I_q^-\right)^* \tag{30}$$

$$Q_i^* = V^-\left(I_p^+\right)^* - V^+\left(I_p^-\right)^*. \tag{31}$$

The voltage V_{max} can be calculated by applying (23)-(31) to its definition in (9). Fig. 5 shows this factor as a function of the control parameter k for two power production scenarios. The values of the DG system used in this figure correspond to those used in the experimental setup described in the next section, which are listed in Table 2. From the figure, it is clear that V_{max} exceeds the upper limit 1.1 p.u. for a range of k that varies according to the power production. In particular, the overvoltage problem is noticed for $-1 \le k \le 0.45$ when P_G = 500 W. Note that the range gets narrower, $-1 \le k \le -0.33$, for P_G = 1500 W. This is because, in high power production scenarios, the reactive current is the minimum value specified by the grid code, as shown in Fig. 3 (see point B). This minimum injection of reactive current results in lower V_{max}, as predicted by (23)-(25). On the contrary, the reactive current takes the maximum value in the lowest power production scenario (see Fig. 3). Therefore, from the point of view of the overvoltage problem, this is the worst case condition.

Table 2 Nominal values of the experimental setup

Symbol	Quantity	Nominal value
V_g	Grid voltage (ph-to-neutral, base voltage)	155 V (peak)
V_g^+	Positive-sequence voltage during the sag	93 V (0.60 p.u.)
V_g^-	Negative-sequence voltage during the sag	70 V (0.45 p.u.)
φ	Initial phase angle between sequences	-30º
ω	Grid angular frequency	2π 60 rad/s
L_g	Grid inductance	4.6 mH (0.11 p.u.)
I_{rated}	Rated inverter current (base current)	10 A (peak)
V_{dc}	Dc-link voltage	350 V
f_s	Switching and sampling frequency	10 kHz

The previous analysis revealed the properties of the proposed control in terms of voltage support. An accurate knowledge of the DG system is necessary for this analysis. For instance, see the numerical value of L_g in Table 2. However, the operation of the proposed control does not need this knowledge, as it can be seen in the pseudocode of Fig. 4.

5 Closed-loop control to avoid overvoltage

This Section presents a voltage regulator that avoids the overvoltage problem according to the control objective 4. It also includes control design guidelines. This is the third contribution of this paper.

5.1 Voltage regulator

The main goal of the regulator is to compensate the increase in V_{max} by increasing the value of k. This action will result in a reduction of V_{max}, as it can be seen in Fig. 5. This strategy can be implemented using a slope voltage control, which is based on a linear relation between its input and output control signals (measured voltage and reference reactive current, respectively) [34, 35]. In addition, a saturation region should be considered to apply the voltage regulation only in the region of interest. All these ideas come together in the control proposed in Fig. 6, which relates measured voltage V_{max} with control parameter k. The proposed slope voltage control can be written as

$$k = \begin{cases} k_H & V_{max} \ge V_H \\ k_L + \dfrac{k_H - k_L}{V_H - V_L}(V_{max} - V_L) & V_L < V_{max} < V_H \\ k_L & V_{max} \le V_L \end{cases} \tag{32}$$

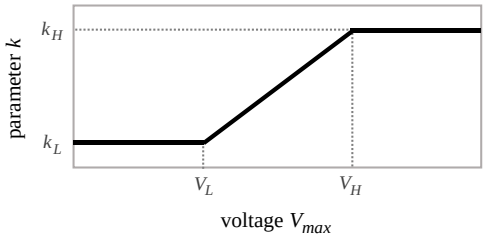

Fig. 6 *Slope voltage control for overvoltage prevention*

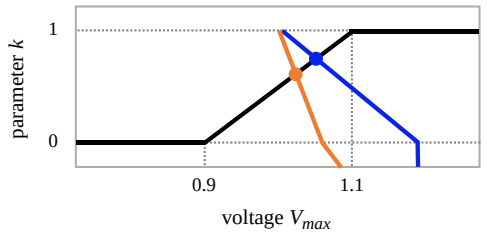

Fig. 7 *Operating points of the proposed slope voltage control for two values of P_G*
(blue) 500 W, ***(orange)*** 1500 W

where (V_L, k_L) and (V_H, k_H) are the coordinates of the two points located at the ends of the linear region.

5.2 Design guidelines

From Fig. 5, it is clear that the overvoltage problem is avoided for high values of k. For this reason, it is recommended to choose k_H as high as possible, then $k_H = 1$. For the design of k_L, there is some degree of freedom. However, the value $k_L = 0$ is recommended to operate the DG system with balanced current when there is no voltage sag. In addition, the voltage parameters are chosen as $V_H = 1.1V_g$ and $V_L = 0.9V_g$ in accordance with the voltage limits in normal conditions [11]. With this design, the range $-1 \leq k < 0$ is not allowed in closed-loop operation due to the saturation region below to the value $V_{max} = 0.9$ p. u.; see Fig. 7.

In closed-loop operation, the operating points of the system are located at intersections of the system and control lines shown in Fig. 5 and 6. For clarity, these points are represented in Fig. 7. Note that the voltage V_{max} is always lower than 1.1 p.u., avoiding the overvoltage problem observed in Fig. 5. The range of values of k is $0.65 \leq k \leq 0.78$.

In Fig. 7, the slope of the system lines (blue and orange) depends on the grid impedance L_g; see (23)-(25). For lower values of L_g, the slope of both lines increases what brings the operating points closer and, as a consequence, the range of k is reduced. Therefore, the proposed control continues to work correctly in scenarios with low L_g.

6 Experimental validation

This section validates the theoretical contributions of this paper. To this end, selected experimental results are reported and discussed in detail below.

6.1 Laboratory setup

The laboratory setup of the three-phase DG system shown in

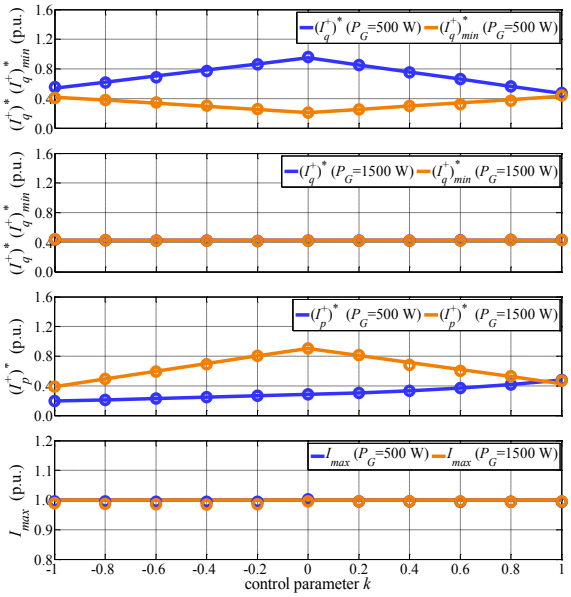

Fig. 8 *Theoretical (continuous lines) and experimental (marked by the symbols o) results of current amplitudes and maximum current for two values of P_G*

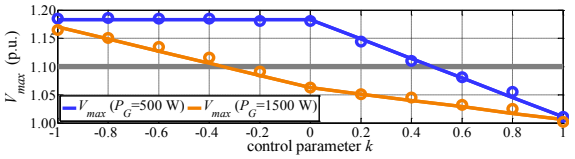

Fig. 9 *Theoretical and experimental results of the maximum amplitude of the phase voltages for two values of P_G*

Fig. 1a is composed of the following components: an AMREL SPS800-12-D013 DC power source, a Guasch MTL-CBI0060-F12IXHF three-phase inverter, a Pacific Power programmable AC power source, and a Texas Instruments dual-core F28M36 floating point DSP. This setup emulates a real scenario in which the DG system is connected to the transmission grid through overhead lines [23]. In this scenario, the impedance is dominantly inductive and L_g takes into account the impedance of both the overhead lines and the transmission grid. The value considered for L_g (0.11 p.u.) is in the typical range for this application [8, 15].

The voltage sag was programmed in the AC power source. It is a single phase-to-ground fault, occurred in some point of the overhead lines [23]. The transmission network voltage v_g is characterized during the fault by the values of V_g^+, V_g^- and φ listed in Table 2.

The control scheme in Fig. 1b was programmed in the C28 processor of the DSP, including the code of the flexible oscillating-power control (see Fig. 4). The M3 processor was used to send inverter measurements to a personal computer for monitoring purposes. The figures with experimental results shown in this section were drawn in MATLAB using these measurements.

Two sets of experimental tests were carried out in the laboratory. The first one evaluated the characteristics of the proposed control strategy, setting the value of k in open loop.

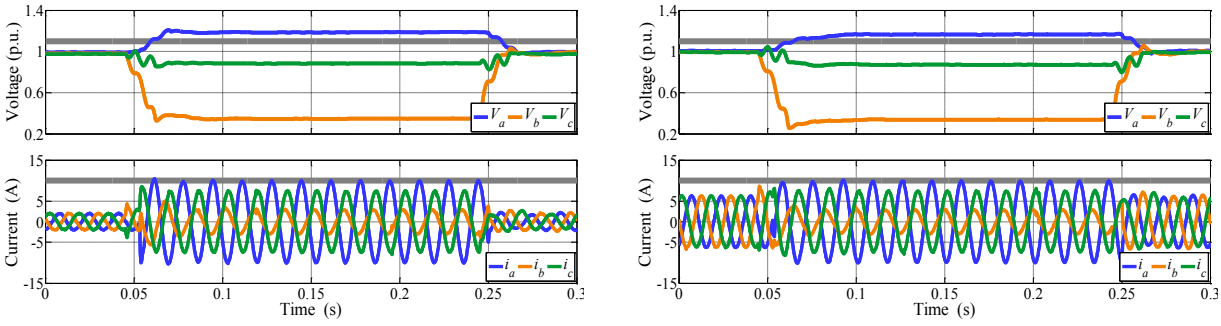

Fig. 10 *Experimental results for the control parameter* $k = -1$
(a) $P_G = 500$ W, ***(b)*** $P_G = 1500$ W

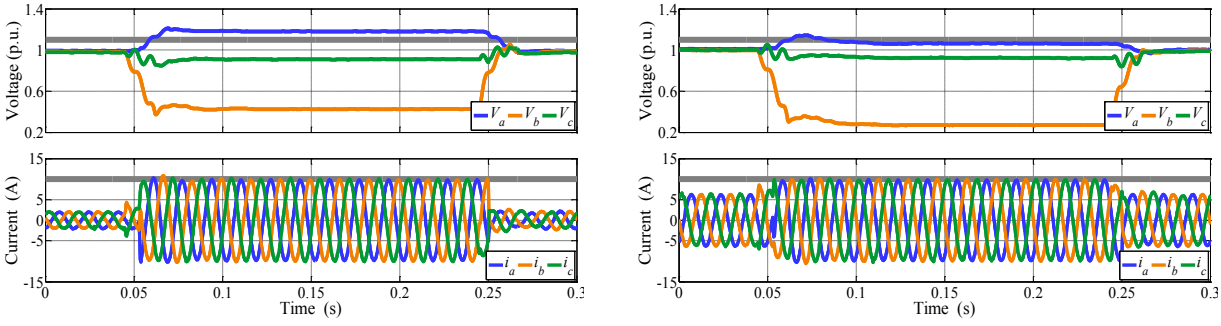

Fig. 11 *Experimental results for the control parameter* $k = 0$
(a) $P_G = 500$ W, ***(b)*** $P_G = 1500$ W

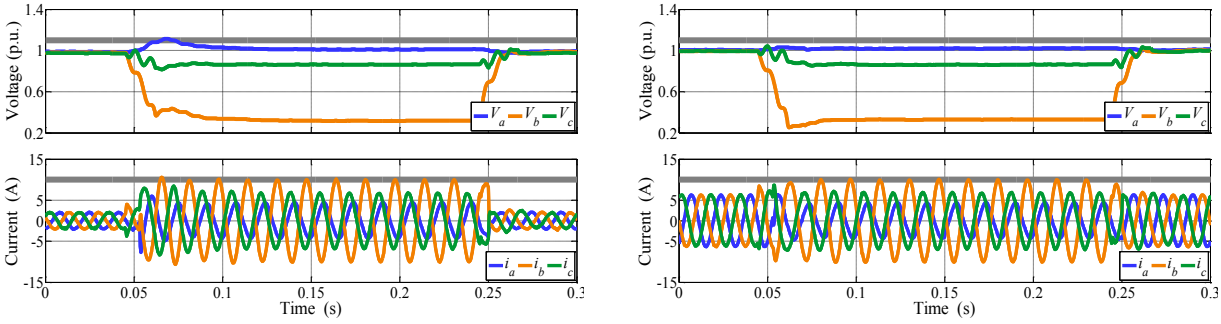

Fig. 12 *Experimental results for the control parameter* $k = 1$
(a) $P_G = 500$ W, ***(b)*** $P_G = 1500$ W

The second one evaluated the performance of the slope voltage control, by coding (32) in the algorithm shown in Fig. 4 (just before line 15). The value of V_{max} was calculated using (9) and (39)-(41).

6.2 Open-loop operation

Fig. 8 verifies the fulfilment of the grid code requirements for current injection. First, the current takes its maximum value for all values of *k*, as stated in (10); see bottom sub-figure. This condition and the produced power affect the active and reactive currents. For low power ($P_G = 500$ W), the active current is low and the reactive current high. This last current is even higher than the minimum current specified by the grid code; see top sub-figure. For high power ($P_G = 1500$ W), the active power curtailment is activated and the reactive current coincides with the minimum value; see middle up sub-figure. Even with the curtailment, the active current is high in this high power production scenario; see middle down sub-figure.

Fig. 9 validates the theoretical results shown in Fig. 5. The overvoltage problem is clearly observed when the maximum voltage V_{max} is higher than the upper voltage limit 1.1 p.u., marked in the figure with a gray solid line.

Fig. 10 to 12 shows the transient response of the DG system for different constant values of *k*. In all these tests, the voltage sag starts at $t = 0.047$ s and is cleared at $t = 0.25$ s. The transient response is strongly dominated by the dynamics of the voltage sequence extractor; see Fig. 1b. Interested readers can consult [27, 28] to find a detailed analysis on the dynamics of the voltage sequence extractor.

Fig. 10 shows the results for $k = -1$. The most significant characteristics are maintained for the two power

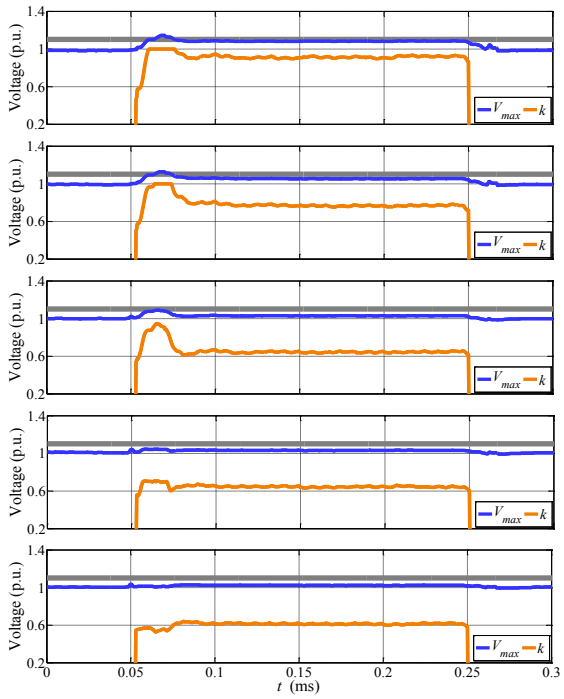

Fig. 13 *Experimental results of the slope voltage control*
From top to bottom: $P_G = 0$ W, 500 W, 1000 W, 1500 W, 2000 W

production scenarios: the maximum voltage exceeds the permitted limit and the maximum current (in phase *a*) coincides with that specified by the grid code. Fig. 11 shows the results for $k = 0$. In this case, the current is balanced, the voltage exceeds its limit when the power is low and is below the limit when the power is high. Finally, Fig. 12 shows the results for $k = 1$. This value of k avoids the overvoltage problem while limiting the maximum current of the system (phase *b* in this case).

6.3 Closed-loop operation

Fig. 12 validates the operation and performance of the slope voltage control. In this test, five power production scenarios were considered. As predicted, the worst case condition is $P_G = 0$; see top sub-figure. In this case, the maximum current is reached only with reactive current (the active current is 0), which causes the highest maximum voltage of all tests. Even in this condition, the design of the voltage control ensures that the maximum voltage does not exceed its upper limit. It is also interesting to see in the figure the different values of k provided by the closed-loop operation of the proposed control. These results agree with the theoretical values shown in Fig. 7.

7 Comparison with other control schemes

Table 3 compares the characteristics of the proposed control with those of the state-of-the-art control solutions. As it was experimentally shown in the previous Section, the proposed control satisfies the reactive current injection requirements of a specific grid code, limits the maximum current of the DG system to the rated current of the inverter, maintains the injection of active power during the voltage sag and prevents overvoltage problems. Most of the state-of-the-art control solutions listed in Table 3 have some of these characteristics, but only the control in [21] achieves all four characteristics simultaneously. However, the proposed control provides a flexible operation with adjustable characteristics by selecting the value of *k*. This is not the case in the control in [21] which has a more rigid operation with fixed characteristics.

Another interesting point for comparison is the practical application of the controls in grids with different impedance ratios. Most of the control schemes are designed for high- to medium voltage grids with dominant inductive impedance, including the proposed control. The control in [36] is devised for low-voltage grids with dominant resistive impedance. What is even more interesting is the ability of the control schemes [9], [26] and [33] to achieve their control objectives regardless of the grid impedance ratio considered. The improvement of the proposed control based on its application to grids with any impedance ratio is an open research topic that is left for a future work.

8 Conclusion

This paper has presented a control scheme to avoid overvoltage problems in three-phase DG systems during

Table 3 Comparison of control schemes designed to operate during voltage sags

Control	Grid code fulfilment	Overcurrent limitation	Active power injection	Overvoltage limitation	Flexibility	Grid impedance
[1, 2, 17, 19]	YES	YES	YES	no	no	Not specified
[3, 4]	no	no	YES	no	no	Not specified
[18, 24]	no	YES	YES	no	no	Not specified
[25]	YES	no	YES	no	no	Not specified
[9]	YES	YES	YES	no	no	Any value
[26]	no	YES	YES	YES	no	Any value
[33]	no	YES	YES	no	no	Any value
[36]	no	no	YES	no	YES	$X/R \ll 1$
[5]	no	no	YES	no	YES	$X/R \gg 1$
[8]	no	YES	YES	YES	no	$X/R \gg 1$
[14, 15]	no	YES	YES	no	no	$X/R \gg 1$
[16]	YES	YES	YES	no	no	$X/R \gg 1$
[20]	no	no	YES	no	no	$X/R \gg 1$
[21]	YES	YES	YES	YES	no	$X/R \gg 1$
[23]	YES	YES	no	no	no	$X/R \gg 1$
[37]	no	YES	YES	no	YES	$X/R \gg 1$
Proposed	YES	YES	YES	YES	YES	$X/R \gg 1$

voltage sags. The scheme is based on combining an advanced version of the flexible oscillating-power control with a slope voltage control. In addition to avoiding overvoltage, the control scheme ensures compliance with the grid-code requirements for current injection and includes a peak-current limitation mechanism. The theoretical contributions of this paper have been experimentally validated in a laboratory prototype. It has been shown by this experimental validation that the proposed control incorporates all the desired characteristics specified by the control objectives.

9 Acknowledgments

This work was supported by the Ministry of Science, Innovation and Universities of Spain and by the European Regional Development Fund under project RTI2018-100732-B-C22.

10 References

[1] Tang, C., Chen, Y.T., Chen, Y.: 'PV power system with multi-mode operation and low-voltage ride-through capability', *IEEE Trans. Ind. Electron.*, 2015, **62**, (12), pp. 7524-7533

[2] Chen, H.C., Lee, C.T., Cheng, P.T., Teodorescu, R., Blaabjerg, F.: 'A low-voltage ride-through technique for grid-connected converters with reduced power transistors stress', *IEEE Trans. Power Electron.*, 2016, **31**, (12), pp. 8562-8571

[3] Rodriguez, P., Timbus, A.V., Teodorescu, R., Liserre, M., Blaabjerg, F.: 'Reactive power control for improving wind turbine system behavior under grid faults', *IEEE Trans. Power Electron.*, 2009, **24**, (7), pp. 1798-1801

[4] Junyent-Ferré, A., Gomis-Bellmunt, O., Green, T.C., Soto-Sánchez, D.E.: 'Current control reference calculation issues for the operation of renewable source grid interface VSCs under unbalanced voltage sags', *IEEE Trans. Power. Electron.*, 2011, **26**, (12), pp. 3744-3753

[5] Wang, F., Duarte, J.L., Hendrix, M.A.: 'Pliant active and reactive power control for grid-interactive converters under unbalanced voltage dips', *IEEE Trans. Power. Electron.*, 2011, **26**, (5), pp. 1511-1521

[6] Tafti, H.D., Maswood, A.I., Lim, Z., Ooi, G.H.P., Raj, P.H.: 'A review of active/reactive power control strategies for PV power plants under unbalanced grid faults', IEEE Innov. Smart Grid Technol.-Asia Conf., Nov. 2015, pp. 1–6

[7] Jia, J., Yang, G., Nielsen, A.H.: 'A review on grid-connected converter control for short circuit power provision under grid unbalanced faults', *IEEE Trans. Power Deliv.*, 2018, **33**, (2), pp. 649-661

[8] Shabestary, M.M., Mohamed, Y.A.: 'Asymmetrical ride-through and grid support in converter-interfaced DG units under unbalanced conditions', *IEEE Trans. Ind. Electron.*, 2019, **66**, (2), pp. 1130-1141

[9] Iglesias Brandao. D., Mendes, F., Vagner Ferreira, R., Magalhaes Silva, S., Amariz Pires, I.: 'Active and reactive power injection strategies for three-phase four-wire inverters during symmetrical/asymmetrical voltage sags', *IEEE Trans. Ind. Applic.*, 2019, **55**, (3), pp. 2347-2355

[10] E.ON Netz GmbH: 'Grid code - High and extra high voltage', Germany, 2006.

[11] Red Eléctrica de España (REE): 'Resolution P.O. 12.3 - Response requirements against voltage dips in wind installations', Spain, 2006

[12] EnergiNet: 'Technical regulation 3.2.5 for wind plants above 11 kW', Denmark, 2016

[13] European Network of Transmission System Operator (ENTSO): 'Network code-requirements for grid connection of generators', Belgium, 2016

[14] Mahamedi, B., Eskandari, M., Fletcher, J.E., Zhu, J.: 'Sequence-based control strategy with current limiting for the fault ride-through of inverter-interfaced distributed generators', *IEEE Trans. Sustain. Energy*, 2020, **11**, (1), pp. 165-174

[15] Huang, L., Xin, H., Wang, Z., Zhang, L., Wu, K., Hu, J.: 'Transient stability analysis and control design of droop-controlled voltage source converters considering current limitation', *IEEE Trans. Smart Grid*, 2019, **10**, (1), pp. 578-591

[16] Lee, C., Hsu, C., Cheng, P.: 'A low-voltage ride-through technique for grid-connected converters of distributed energy resources', *IEEE Trans. Ind. Appl.*, 2011, **47**, (4), pp. 1821-1832

[17] Nasiri, M., Mohammadi, R.: 'Peak current limitation of grid side inverter by limited active power in PMSG-based wind turbines during different grid faults', *IEEE Trans. Sustain. Energy*, 2017, **8**, (1), pp. 3-12

[18] Tafti, H.D., Maswood, A.I., Konstantinou, G., Pou, J., Acuna, P.: 'Active/reactive control of photovoltaic grid-tied inverters with peak current limitation and zero active power oscillation during unbalanced voltage sags', *IET Power Electron.*, 2018, **11**, (6), pp. 1066-1073

[19] Garnica, M.A., García de Vicuña, L., Miret, J., Castilla, M., Guzmán, R.: 'Control strategy for grid-connected three-phase inverters during voltage sags to meet grid codes and to maximize power delivery capability', *IEEE Trans. Power Electron.*, 2018, **33**, (11), pp. 9360-9374

[20] Ma, K., Chen, W., Liserre, M., Blaabjerg, F.: 'Power controllability of a three-phase converter with an unbalanced AC source', *IEEE Trans. Power Electron.*, 2015, **30**, (3), pp. 1591-1604

[21] Mirhosseini, M., Pou, J., Agelidis, V.G.: 'Individual phase current control with the capability to avoid overvoltage in grid-connected photovoltaic power plants under unbalanced voltage sags', *IEEE Trans. Power Electron.*, 2015, **30**, (10), pp. 5346-5351

[22] Masters, C.L.: 'Voltage rise: The big issue when connecting embedded generation to long 11 kV overhead lines', *Inst. Elect. Power Eng. J.*, 2002, **16**, (1), pp. 5-12

[23] Goksu, O., Teodorescu, R., Bak, C.L., Iov, F., Kjaer, P.C.: 'Impact of wind power plant reactive current injection during asymmetrical grid faults', *IET Renew. Power Gener.*, 2013, **7**, (5), pp. 484-492

[24] Milicua, A., Abad, G., Vidal, M.R.: 'Online reference limitation method of shunt-connected converters to the grid to avoid exceeding voltage and current limits under unbalanced operation; Part I: Theory," *IEEE Trans. Energy Convers.*, 2015, **30**, (3), pp. 852-863

[25] Uphues, A., Notzold, K., Wegener, R., Soter, S., Griessel, R.: 'Support of grid voltages with asymmetrical reactive currents in case of grid errors', IEEE Int. Conf. Ind. Technol., Feb. 2013, pp. 1781-1786

[26] Shabestary, M.M., Mohamed, Y.A.I.: 'Advanced voltage support and active power flow control in grid-connected converters under unbalanced conditions', *IEEE Trans. Power Electron.*, 2018, **33**, (2), pp. 1855-1864

[27] Rodriguez, F.J., Bueno, E., Aredes, M., Rolim, L.G., Neves, F.A., Cavalcanti, M.C.: 'Discrete-time implementation of second-order generalized integrators for grid converters', 34th Annu. Conf. IEEE Ind. Electron., Nov. 2008, pp. 176-181

[28] Rodriguez, P., Luna, A., Candela, I., Mujal, R., Teodorescu, R., Blaabjerg, F.: 'Multiresonant frequency-locked loop for grid synchronization of power converters under distorted grid conditions," 2011, *IEEE Trans. Ind. Electron.*, **58**, (1), pp. 127-138

[29] Bojoi, R.I., Griva, G., Bostan, V., Guerreiro, M., Farina, F., Profumo, F.: 'Current control strategy for power conditioners using sinusoidal signal integrators in synchronous reference frame', *IEEE Trans. Power Electron.*, 2005, **20**, (6), pp. 1402-1412

[30] Liserre, M., Teodorescu, R., Blaabjerg, F.: 'Multiple harmonics control for three-phase grid converter systems with the use of PI-RES current controller in a rotating frame', *IEEE Trans. Power Electron.*, 2006, **21**, (3), pp. 836-841

[31] Tsili, M., Papathanassiou, S.: 'A review of grid code technical requirements for wind farms', *IET Renew. Power Gener.*, 2009, **3**, (3), pp. 308-332

[32] Altin, M., Goksu, O., Teodorescu, R., Rodriguez, P., Bak-Jensen, B., Helle, L.: 'Overview of recent grid codes for wind power integration', *12th Int. Conf. Optim. Electr. Electron. Equip.*, May 2010, pp. 1152-1160

[33] Camacho, A., Castilla, M., Miret, J., García de Vicuña, L., Garnica López, M.A.: 'Control strategy for distribution generation inverters to maximize the voltage support in the lowest phase during voltage sags', *IEEE Trans. Ind. Electron.*, 2018, **65**, (3), pp. 2346-2355

[34] Martinez, J., Kjr, P.C., Rodriguez, P., Teodorescu, R.: 'Design and analysis of a slope voltage control for a DFIG wind power plant', *IEEE Trans. Energy Convers.*, 2012, **27**, (1), pp. 11-20

[35] Rey, J.M., Castilla, M., Miret, J., Camacho, A., Guzman, R.: 'Adaptive slope voltage control for distributed generation inverters with improved transient performance', *IEEE Trans. Energy Convers.*, 2019, **34**, (3), pp. 1644-1654

[36] Guo, X., Zhang, B., Wu, W, Guerrero, J.M.: 'Asymmetrical grid fault ride-through strategy of three-phase grid-connected inverter

considering network impedance impact in low-voltage grid', *IEEE Trans. Power Electron.*, 2014, **29**, (3), pp. 1064-1068

[37] Camacho, A., Castilla, M., Miret, J., Borrell, A., Garcia de Vicuña, L.: 'Active and reactive power strategies with peak current limitation for distributed generation inverters during unbalanced grid faults', *IEEE Trans. Ind. Electron.*, 2015, **62**, (3), pp. 1515-1525

11 Appendix

This appendix derives the amplitudes of the reference reactive phase currents as a function of the amplitudes of the reference sequence currents.

In a three-phase system, the reference reactive phase powers are defined as [37]

$$q_x^* = v_x^{\perp} i_x^* \tag{33}$$

where *x* stands for phases *a*, *b*, and *c*, $v_x^{\perp}$ are the in-quadrature components of the phase voltages, and i_x^* are the reference phase currents. The reactive powers in (33) can be separated in quiescent and oscillating terms [4, 36]. The quiescent terms can be written as a function of the reference reactive phase currents as

$$Q_x^* = \frac{V_x I_{qx}^*}{2}. \tag{34}$$

The procedure to derive the reactive currents in (34) is presented below:

1) Write the sequence voltages in the $\alpha\beta$ reference frame

$$v_\alpha^+ = V^+ \cos(\omega t) \tag{35}$$

$$v_\beta^+ = V^+ \sin(\omega t) \tag{36}$$

$$v_\alpha^- = V^- \cos(-\omega t - \varphi) \tag{37}$$

$$v_\beta^- = V^- \sin(-\omega t - \varphi). \tag{38}$$

   Note that the initial phase of the positive-sequence voltages is set to 0. This can be assumed without loss of generality by inserting the initial phase φ into the negative-sequence voltages.
2) From (35)-(38), calculate $v_x^{\perp}$ by using the inverse Clarke's transformation and introducing a phase delay of $-\pi/2$ in the initial phase of the resulting expressions.
3) Obtain i_x^* by inserting (35)-(38) into (1)-(2) and using the inverse Clarke's transformation.
4) Insert $v_x^{\perp}$ and i_x^* in (33) and identify the quiescent terms of the reference reactive powers.
5) With (34) and the results of the previous step, the amplitudes of the reference reactive phase currents are obtained. These expressions are written in (26)-(28).

Additionally, the amplitude of the phase voltages can be obtained from (35)-(38) as

$$V_a = \sqrt{(V^+)^2 + (V^-)^2 + 2V^+V^- \cos\varphi} \tag{39}$$

$$V_b = \sqrt{(V^+)^2 + (V^-)^2 + 2V^+V^- \cos(\varphi - 2\pi/3)} \tag{40}$$

$$V_c = \sqrt{(V^+)^2 + (V^-)^2 + 2V^+V^- \cos(\varphi + 2\pi/3)}. \tag{41}$$